arXiv:1408.4326v2 [cond-mat.mtrl-sci] 3 Sep 2014

Stroboscopic detection of nuclear resonance in an arbitrary scattering channel

L. Deák,[a]* L. Bottyán,[a] R. Callens,[b] R. Coussement,[b1] M. Major,[c2] S. Nasu,[d3] I. Serdons,[b] H. Spiering[e] and Y. Yoda[f]

[a] *Wigner RCP, RMKI, P.O.B. 49, 1525 Budapest, Hungary,* [b] *Instituut voor Kern- en Stralingsfysica, K.U.Leuven, Celestijnenlaan 200D, B-3001 Leuven, Belgium,* [c] *Institute for Materials Science, Technische Universität Darmstadt, 64287 Darmstadt, Germany,* [d] *Grad. School of Eng. Sci., Osaka Univ., Toyonaka, Osaka 560-8531, Japan,* [e] *Institut für Anorganische und Analytische Chemie, Johannes Gutenberg Universität Mainz, Staudinger Weg 9, D-55099 Mainz, Germany, and* [f] *SPring-8 JASRI, 1-1-1 Kouto, Mikazuki-cho, Sayo-gun, Hyogo 679-5198, Japan.*

E-mail: deak.laszlo@wigner.mta.hu

nuclear resonant scattering; stroboscopic detection; multilayer

Abstract

The theory of heterodyne/stroboscopic detection of nuclear resonance scattering is developed, starting from the total scattering matrix as a product of the matrix of the reference sample and the sample under study. This general approach holds for any dynamical scattering channel. The forward channel, which is discussed in detail in

[1] Deceased 9 July 2012
[2] On leave from Wigner RCP, RMKI, P.O.B. 49, 1525 Budapest, Hungary
[3] Deceased 16 April 2014

the literature, reveals the speciality that electronic scattering causes only an energy independent diminution of the intensity. For all other channels, complex resonance line shapes in the heterodyne/stroboscopic spectra—as a result of interference of electronic and nuclear scattering—is encountered. The grazing incidence case is evaluated and described in detail. Experimetal data of classical grazing incidence reflection and their stroboscopic detection on $\left[^{\rm nat}{\rm Fe}/^{57}{\rm Fe}\right]_{10}$ and antiferromagnetic $\left[^{57}{\rm Fe}/{\rm Cr}\right]_{20}$ multilayers are fitted simultaneously.

1. Introduction

Nuclear resonant scattering (NRS) of synchrotron radiation (SR) has become an established method for the study of nuclear hyperfine interaction during the last two decades (Gerdau & DeWaard, 1999; Röhlsberger, 2005). The spectrum is conventionally recorded as the time response of the nuclear ensemble following a short resonant synchrotron pulse, which simultaneously excites all resonant transitions between hyperfine-split nuclear sublevels. The observed beating frequencies are characteristic for the hyperfine fields in the specimen. As an alternative to nuclear resonant forward scattering of SR in time domain, a heterodyne detection scheme was suggested (Coussement *et al.*, 1996; L'abbé *et al.*, 2000). The two scatterers, viz. the one under investigation and as a reference sample a single-line Mössbauer absorber, are mounted on a Mössbauer drive. The heterodyne spectrum is the full time integral of the delayed counts, plotted as a function of the Doppler velocity of the reference sample. An advantage of this experimental setup is the similarity of the spectra to those in the conventional energy-domain Mössbauer spectroscopy (Coussement *et al.*, 1996; L'abbé *et al.*, 2000). Although conventional Mössbauer spectroscopy delivers similar information on hyperfine interactions, the special properties of SR like high collimation, high degree of polarization and high brilliance increase the number of possible applications

of NRS of SR. Furthermore, the heterodyne setup allows for dense bunch modes of the synchrotron (with bunch separation time much shorter than the nuclear lifetime), which are not suitable for time differential NRS experiments.

Undistorted time integration of the nuclear response can only be performed if the large non-resonant intensity contribution is extinguished. Experimentally, this can be achieved by using radiation from a nuclear monochromator (Smirnov *et al.*, 1997) or by applying a polarizer/analizer setup (L'abbé *et al.*, 2000). An alternative approach, namely, "stroboscopic detection", is based on appropriate time gating (Callens *et al.*, 2002; Callens *et al.*, 2003), i.e., integration of the delayed time response in a periodic time window. The period t_p of the observation time window after the SR pulse is chosen so that $1/t_p$ falls within the frequency range of the hyperfine interactions in the investigated specimen. This leads to new type of periodic resonances at certain Doppler velocities that are shifted from the Mössbauer resonances by mh/t_p, with h being Planck's constant, and m an integer number indicating the stroboscopic order (Callens *et al.*, 2002; Callens *et al.*, 2003). The period t_p should be selected according to the hyperfine spectral range, the synchrotron bunch period and the detector dead time (Serdons *et al.*, 2004; Callens *et al.*, 2003).

So far the theory of stroboscopic detection scheme has only been developed and discussed in detail for forward scattering geometry. The several applications of NRS in surface and thin-film magnetism that make use of the grazing incidence geometry (Röhlsberger, 2005; Chumakov *et al.*, 1999; Röhlsberger, 1999; Deák *et al.*, 1999; Röhlsberger *et al.*, 2003; Sladecek *et al.*, 2002) call for computer programs that easily allow to fit data obtained by stroboscopic detection as well. In this geometry, the interferences of the SR plane waves, scattered from the surface and interfaces of a stratified sample, provide information on the value, direction and topology of the internal fields in the sample with nanometer depth resolution.

Recently, interesting experiments have been performed using stroboscopic detection in the grazing incidence case (Röhlsberger *et al.*, 2010; Röhlsberger *et al.*, 2012), which demonstrates the potential of this method.

Grazing-incident NRS of SR, often called Synchrotron Mössbauer Reflectometry (SMR) (Gerdau & DeWaard, 1999; Deák *et al.*, 2001; Deák *et al.*, 2002), has been established in both time and angular regime (Chumakov *et al.*, 1999; Deák *et al.*, 2002; Nagy *et al.*, 1999), as time differential (TD) and time integral (TI) SMR, respectively. In the forward scattering channel, the prompt electronic scattering homogeneously contributes to the stroboscopic spectrum and does not affect the spectral shape. For other scattering channels, including grazing incidence reflection, the interference of the electronic and nuclear scattering provides further information. The stroboscopic SMR line shape may considerably differ from the forward Mössbauer spectrum, calling for a specialized computer code.

The dynamical theory of x-ray scattering gives a self-consistent description of the radiation field in all scattering channels of the system of scatterers, taking all orders of multiple scattering into account. Theories that expand the coherent elastic scattering to the case of sharp nuclear resonances (Afanasev & Kagan, 1964; Kagan & Afanasev, 1964; Hannon & Trammell, 1968; Hannon & Trammell, 1969; Hannon *et al.*, 1985*a*) have been applied to various scattering geometries. The simplest cases are the one-beam cases, such as forward and off-Bragg scattering, and the two-beam cases, the Bragg-Laue scattering (Hannon & Trammell, 1969; Sturhahn & Gerdau, 1994) and the grazing incidence scattering (Röhlsberger *et al.*, 2003; Hannon & Trammell, 1969; Hannon *et al.*, 1985*b*; Irkaev *et al.*, 1993; Deák *et al.*, 1996). In the grazing incidence limit, an optical model was derived from the dynamical theory (Hannon & Trammell, 1969; Hannon *et al.*, 1985*b*), which has been implemented in numerical calculations (Röhlsberger *et al.*, 2003). The reflectivity formulae given by Deák *et al.* (1996) and

Deák *et al.* (2001) are suitable for fast numerical calculations in order to actually fit the experimental data (Spiering *et al.*, 2000) and, as has been shown (Deák *et al.*, 1999), this optical method is equivalent to that of the other approaches in the literature (Röhlsberger *et al.*, 2003; Hannon *et al.*, 1985*b*).

The aim of the present paper is to develop the concept of the heterodyne/stroboscopic detection and to establish the formula that can be applied to any scattering channel, like forward scattering, Bragg, off-Bragg and grazing incidence scattering.

This paper is organized as follows. In the second section, the heterodyne/stroboscopic intensity formula for the propagation of γ–photons in a medium containing both electronic and resonant nuclear scatterers is derived. The equivalence to the previously discussed calculations for the forward channel (Callens *et al.*, 2002; Callens *et al.*, 2003) are shown and the important specific case of the stroboscopic grazing incidence reflection are outlined. In the third section, features of the grazing incidence case are demonstrated by least-squares fitted experimental stroboscopic SMR spectra on isotope-periodic $[^{\rm nat}{\rm Fe}/^{57}{\rm Fe}]$ and antiferromagnetically ordered $[^{57}{\rm Fe}/{\rm Cr}]$ multilayer films.

2. Heterodyne/Stroboscopic detection of Nuclear Resonance Scattering

2.1. General considerations

The setup of a heterodyne/stroboscopic NRS of SR experiment includes two scatterers, the investigated specimen and an additional reference sample (Coussement *et al.*, 1996; L'abbé *et al.*, 2000; Callens *et al.*, 2002; Callens *et al.*, 2003), the latter being mounted on a Mössbauer drive (in forward scattering geometry). The Mössbauer drive provides a Doppler-shift $E_v = (v/c)\,E_0$ of the nuclear energy levels, with c, v and E_0 being the velocity of light, the velocity of the drive and the energy of the Mössbauer transition, respectively. The polarization dependence of the nuclear scat-

terers is described adopting the notation of Sturhahn & Gerdau (1994), by 2×2 transmissivity and reflectivity matrices commonly called *scattering matrices*. The scattering of the synchrotron photons on the specimen and the reference sample is described by the *total scattering matrix* $T_\tau\left(E,E_v\right)$,

$$T_\tau\left(E,E_v\right)=T_\tau^{(\mathrm{s})}\left(E\right)T^{(\mathrm{r})}\left(E-E_v\right), \tag{1}$$

a product of the scattering matrices of the reference sample $T^{(\mathrm{r})}$ and of the investigated specimen $T^{(\mathrm{s})}$ (Blume & Kistner, 1968) in the energy domain. The index τ specifies the open scattering channel (Hannon & Trammell, 1969; Sturhahn & Gerdau, 1994). The scattering matrix $T^{(\mathrm{r})}\left(E-E_v\right)$ of the reference sample depends on the Doppler-shifted energy $E-E_v$, where the channel index τ is omitted for forward scattering. Note that both the electrons and the resonant Mössbauer nuclei scatter the γ–photons coherently so the scattering matrices have a resonant nuclear and nearly energy-independent electronic contribution. At energies being far from the Mössbauer resonances ($E\rightarrow\pm\infty$) on a hyperfine scale, the individual scattering matrices $T^{(\mathrm{s,r})}\left(E\rightarrow\pm\infty\right)$, and thus their product $T_\tau\left(E\rightarrow\infty,E_v\right)\equiv T_{\tau,\infty}$ in Eq. (1), approach the non-resonant electronic contribution:

$$T_{\tau,\infty}=T_{\tau,\mathrm{el}}^{(\mathrm{s})}T_{\mathrm{el}}^{(\mathrm{r})}. \tag{2}$$

Since the reference is mounted in forward geometry, its scattering matrix $T^{(\mathrm{r})}\left(E\right)$ is the matrix exponential

$$T^{(\mathrm{r})}\left(E\right)=\exp\left[ikd^{(\mathrm{r})}n^{(\mathrm{r})}\left(E\right)\right], \tag{3}$$

where $n^{(\mathrm{r})}\left(E\right)$ is the index of refraction, $d^{(\mathrm{r})}$ the thickness and k the vacuum wave number of the incident radiation (Blume & Kistner, 1968; Lax, 1951). The index of refraction is related to the susceptibility matrix χ (Deák *et al.*, 2001; Deák *et al.*, 1996) through

$$n^{(\mathrm{r})}\left(E\right)\equiv I+\frac{\chi^{(\mathrm{r})}\left(E\right)}{2}, \tag{4}$$

where I is the unit matrix and $\chi^{(\mathrm{r})} = \frac{4\pi N^{(\mathrm{r})}}{k^2} f^{(\mathrm{r})}$, with $N^{(\mathrm{r})}$ and $f^{(\mathrm{r})}$ being the density of the scattering centers and the 2×2 coherent forward scattering amplitude (Blume & Kistner, 1968), respectively. The susceptibility is the sum of the electronic and the nuclear susceptibilities,

$$\chi^{(\mathrm{r})}(E) = \chi^{(\mathrm{r})}_{\mathrm{el}} + \chi^{(\mathrm{r})}_{\mathrm{nuc}}(E). \tag{5}$$

With Eqs. (3), (4) and (5), the transmissivity of the reference is expressed as a product of electronic and nuclear transmissivities,

$$T^{(\mathrm{r})}(E) = T^{(\mathrm{r})}_{\mathrm{el}} \tilde{T}^{(\mathrm{r})}_{\mathrm{nuc}}(E), \tag{6}$$

where

$$\tilde{T}^{(\mathrm{r})}_{\mathrm{nuc}}(E) = \exp\left(ikd^{(\mathrm{r})} \frac{\chi^{(\mathrm{r})}_{\mathrm{nuc}}(E)}{2}\right). \tag{7}$$

$T^{(\mathrm{s})}_{\tau}(E)$ is determined from the respective theory of wave propagation of channel τ (forward, Bragg-Laue, grazing incidence, etc. scattering), i.e., from the dynamical theory (Hannon & Trammell, 1968; Hannon & Trammell, 1969; Hannon *et al.*, 1985*a*; Sturhahn & Gerdau, 1994; Hannon *et al.*, 1985*b*).

In forward scattering, due to the exponential expression in (3), the total transmissivity $T(E, E_v) = T_\infty \tilde{T}^{(\mathrm{r})}_{\mathrm{nuc}}(E - E_v)\, \tilde{T}^{(\mathrm{s})}_{\mathrm{nuc}}(E)$ is proportional to T_∞. Therefore, in this special case, the electronic scattering is a simple multiplicative factor, which does not affect the spectral shape.

The intensity I_τ allowing for a general polarization state of the incident beam, the 2×2 polarization density matrix ρ (Blume & Kistner's (1968)), is given by

$$I_\tau(E, E_v) = \mathrm{Tr}\left[T^{\dagger}_{\tau}(E, E_v)\, T_\tau(E, E_v)\, \rho\right]. \tag{8}$$

The beating time response to a single short polychromatic photon bunch of SR is obtained by the Fourier transform of the energy domain scattering matrices (Gerdau & DeWaard, 1999; Hannon *et al.*, 1985*a*),

$$T_\tau(t, E_v) = \frac{1}{\sqrt{2\pi}\hbar} \int \mathrm{d}E\, \left[T_\tau(E, E_v) - T_{\tau,\infty}\right] \exp\left(-i\frac{E}{\hbar}t\right), \tag{9}$$

where, by subtracting the constant $T_{\tau,\infty}$, the Dirac delta–like prompt ($t = 0$) and the delayed ($t > 0$) time responses are separated (Sturhahn & Gerdau, 1994). We note that Eq. (9) is valid only for delayed times $t > 0$ after the SR bunch ($t = 0$), but $T_\tau(t, E_v) = 0$ for $t < 0$! In the same way as for Eq. (8), the delayed intensity in time domain becomes

$$I_\tau(t, E_v) = \mathrm{Tr}\left[T_\tau^\dagger(t, E_v)\, T_\tau(t, E_v)\, \rho\right]. \tag{10}$$

For a heterodyne/stroboscopic NRS of SR experiment a time window function is introduced, which can be described by boxcar functions, namely, $S(t) = 1$ for $mt_\mathrm{B} + t_1 < t < mt_\mathrm{B} + t_2$ and $S(t) = 0$ otherwise, with a time interval t_B between the synchrotron bunches and an integer number m. The periodic time window function is expanded in Fourier series,

$$S(t) = \sum_{-\infty}^{\infty} s_m \exp(im\Omega t), \tag{11}$$

where $\Omega = \frac{2\pi}{t_\mathrm{B}}$ is the angular frequency of the SR bunches (Callens *et al.*, 2002; Callens *et al.*, 2003).

The total delayed photon rate $D_\tau(E_v)$ of one bunch is

$$D_\tau(E_v) = \int_{-\infty}^{\infty} \mathrm{d}t\, S(t)\, I_\tau(t, E_v), \tag{12}$$

the integral of the intensity $I_\tau(t, E_v)$ times $S(t)$. Since there is no coherence between photons generated by different electron bunches, the integral of the contribution of one bunch reveals the correct contribution of multiple bunches with periodicity of t_B.

Combining Eqs. (9), (10), (12) and (11), the delayed count rate can be written as

$$D_\tau(E_v) = \sum_{-\infty}^{\infty} s_m \delta_{\tau,m}(E_v), \tag{13}$$

where

$$\delta_{\tau,m}(E_v) = \frac{1}{\hbar}\int \mathrm{d}E \mathrm{Tr}\left\{\left[T_\tau^\dagger(E - m\varepsilon, E_v) - T_{\tau,\infty}^\dagger\right]\left[T_\tau(E, E_v) - T_{\tau,\infty}\right]\rho\right\} \tag{14}$$

and

$$\varepsilon = \hbar\Omega. \tag{15}$$

Since the time window $S(t)$ and the intensity $D_\tau(E_v)$ are real functions, $S_m = S^*_{-m}$ and $\delta_m = \delta^*_{-m}$ hold, and Eq. (13) can be rewritten as

$$D_\tau(E_v) = s_0\delta_{\tau,0} + \sum_{m=1}^{\infty} 2\mathrm{Re}\left(s_m\delta_{\tau,m}\right). \tag{16}$$

The result in Eqs. (13)–(15) is a direct generalization of the intensity formula (8) to the heterodyne/stroboscopic NRS of SR for any observed channel τ in the applied experimental geometry. This expression has already been derived for the case of forward scattering (Callens *et al.*, 2002; Callens *et al.*, 2003). The $m = 0$ term was called the "heterodyne spectrum" (Coussement *et al.*, 1996; Callens *et al.*, 2002), while the $m > 0$ terms were called "stroboscopic resonances" of order m (Callens *et al.*, 2002). Nevertheless, the stroboscopic resonances are not restricted to the forward scattering case. They also appear in other experimental geometries, including, as we show below, in the grazing incidence scattering geometry.

2.2. Grazing incidence geometry

In what follows, stroboscopic SMR spectra will be discussed. In terms of the dynamical theory, grazing incidence is a two-beam case. The $\tau = 0^+$ transmission and the $\tau = 0^-$ reflection channels are open (Röhlsberger, 2005; Hannon & Trammell, 1969; Sturhahn & Gerdau, 1994), the latter being observed in SMR. Close to the electronic total reflection, the reflected intensity is high. Therefore, SMR is an experimentally fairly instructive special case. The reflection from the surface of the specimen is a multiple coherent scattering process of the (SR) photons on atomic electrons and resonant Mössbauer nuclei (Deák *et al.*, 2001; Hannon *et al.*, 1985*b*; Deák *et al.*, 1996). Like in the forward case, this scattering is independent of the atomic positions in the reflecting medium, such that the scattering is described by its index of refraction $n(E)$ (Deák

et al., 1996; Lax, 1951). Henceforth, in compliance with the literature (Röhlsberger *et al.*, 2003; Deák *et al.*, 2001; Deák *et al.*, 1996), in the general theory, the scattering matrix $T_\tau^{(\mathrm{s})}(E)$ will be replaced by the 2×2 reflectivity matrix $R^{(\mathrm{s})}(E,\theta)$, where θ is the angle of incidence. This takes into account the interferences of the reflected radiation from the surfaces and interfaces between the layers with different refraction index. The methods of calculating the reflectivity matrix can be found in the literature (Röhlsberger *et al.*, 2003; Deák *et al.*, 2001; Deák *et al.*, 1996). Accordingly, the total scattering matrix of the specimen and the reference from Eq. (1) is

$$T(E,E_v,\theta) = R^{(\mathrm{s})}(E,\theta)\, T^{(\mathrm{r})}(E-E_v)\,. \tag{17}$$

Similarly, for energies being far from the Mössbauer resonances, Eq. (2) reads

$$T_\infty(\theta) = R_{\mathrm{el}}^{(\mathrm{s})}(\theta)\, T_{\mathrm{el}}^{(\mathrm{r})}. \tag{18}$$

Inserting $T(E,E_v)$ and T_∞ into Eq. (13), the delayed count rate $D(E_v,\theta)$ of the heterodyne/stroboscopic spectrum for grazing incidence (stroboscopic SMR intensity) on the specimen is calculated.

Combining Eqs. (6), (7) and (14) reveal

$$\begin{aligned}\delta_m(E_v,\theta) &= \frac{A^{(\mathrm{r})}}{\hbar}\int \mathrm{d}E \mathrm{Tr}\left\{\left[\tilde{T}^\dagger(E-E_v-m\varepsilon)\, R^\dagger(E-m\varepsilon) - R_{\mathrm{el}}^\dagger\right]\right. \\ &\quad \left.\times\left[R(E)\,\tilde{T}(E-E_v) - R_{\mathrm{el}}\right]\rho\right\},\end{aligned} \tag{19}$$

where $A^{(\mathrm{r})} = \left|T_{\mathrm{el}}^{(\mathrm{r})}\right|^2$ is the electronic absorption of the reference sample. For the sake of simplicity, the indices on the right hand side have been omitted, so that $\tilde{T}_{\mathrm{nuc}}^{(\mathrm{r})} \to \tilde{T}$, $R_{\mathrm{el}}^{(\mathrm{s})}(\theta) \to R_{\mathrm{el}}$ and $R^{(\mathrm{s})}(E,\theta) \to R(E)$. Note that all reflectivities are those of the specimen, and all transmissivities are those of the reference sample. With the relevant angular parameter θ for grazing incidence, Eq. (13) reads

$$D(E_v,\theta) = \sum_{-\infty}^{\infty} s_m \delta_m(E_v,\theta)\,. \tag{20}$$

The observed nuclear, as well as stroboscopic, resonances can be interpreted in a straightforward manner using Eq. (19). Indeed, far from the resonances, $R\,(E \to \infty) = R_{\mathrm{el}}$ and $\tilde{T}\,(E \to \infty) = 1$, and the differences in the square brackets in (19) vanish. We expect a significant contribution to the energy integral only if at least one energy argument of each bracket is close to resonance, i.e., either

$$E - E_v - m\varepsilon \simeq 0 \quad \text{and} \tag{21a}$$

$$E \simeq E_i \tag{21b}$$

or

$$E - m\varepsilon \simeq E_i \quad \text{and} \tag{22a}$$

$$E - E_v \simeq 0 \tag{22b}$$

are fulfilled, where E_i is the energy of the i^{th} Mössbauer resonance of the specimen. The m^{th} term of the sum in Eq. (20) contributes considerably if the Doppler velocity is near to the corresponding shifted Mössbauer resonance. In this case:

$$E_v = E_i - m\varepsilon + \Delta, \tag{23a}$$

$$E_v = E_i + m\varepsilon + \Delta. \tag{23b}$$

Here, Δ is a small deviation (of the order of the resonance line width) from the energy $E_i - m\varepsilon$ or $E_i + m\varepsilon$, ensuring the appearance of stroboscopic resonances also in grazing incidence geometry. In the case of $m = 0$, all four conditions of Eqs. (21) and (22) may be true simultaneously. This means that, for $m = 0$, nuclear scattering in both samples, i.e., "the radiative coupling of the samples" (Callens *et al.*, 2003), also contributes. Hence, the dynamical line broadening (coherent speed-up) is the most effective in the heterodyne spectrum (= baseline and resonances of stroboscopic order 0).

In order to perform computer simulations of stroboscopic spectra, Eqs. (14) and (19) were calculated for the forward scattering and SMR cases, respectively. Eqs. (14),

(19) and (16) were implemented in the evaluation program EFFI (Deák *et al.*, 2001; Spiering *et al.*, 2000). This program allows for least-square fitting of stroboscopic spectra. Moreover, they can be fitted *simultaneously* with other types of spectra of the same specimen, such as forward scattering, grazing incidence, conventional Mössbauer and other spectra of the implemented theory (Deák *et al.*, 2001; Spiering *et al.*, 2000). This way, the fit constraints on the common parameters become very general, as already described (Deák *et al.*, 2001; Spiering *et al.*, 2000).

3. Experimental results and discussion

In order to test the feasibility of this new reflectometric scheme, we investigated two film specimens, a ^{nat}Fe/^{57}Fe isotopic and a ^{57}Fe/Cr antiferromagnetic multilayer, in grazing incidence reflection geometry, using the 14.4 keV Mössbauer transition of ^{57}Fe nuclei. The experiments were performed at the BL09XU nuclear resonance beam line of SPring-8 (Yoda *et al.*, 2001). The experimental setup is shown in Fig. 1. The synchrotron was operated in the 203-bunch mode, corresponding to a bunch separation time of 23.6 ns. The SR was monochromated by a Si(422)/Si(12 2 2) double channel-cut high resolution monochromator with 6 meV resolution. It was incident on the $K_4[^{57}Fe(CN)_6]$ single line pelleted reference sample of effective thickness 11, and on the multilayer specimen downstream mounted in grazing incidence geometry (Fig. 1). The Mössbauer drive was operated in constant acceleration mode, with a maximum velocity of $v_{max} = 20.24$ mm/s. This maximum was calibrated by fitting the velocity separation of the stroboscopic orders in a forward scattering stroboscopic spectrum of a single line ^{57}Fe-enriched stainless steel absorber (Callens *et al.*, 2002; Callens *et al.*, 2003). The delayed radiation was detected using three 2 ns dead time Hamamatsu avalanche photo diodes (APD) in series. To record the delayed intensity, a two-dimensional data acquisition system was used. Each count was indexed according to the time elapsed

after the synchrotron pulse (1024 channels), as well as to the velocity of the reference (1024 channels). These stroboscopic SMR data were time integrated using appropriate time windows of $t_p = 7.87$ ns period and 3.93 ns length (Callens *et al.*, 2002; Callens *et al.*, 2003). Since the energy is measured in mm/s, the shift of the first stroboscopic order, Eq. (15), can be rewritten as

$$\varepsilon \ \ [\mathrm{mm/s}] = 1000 \frac{\lambda \ \ [\mathrm{nm}]}{t_p \ \ [\mathrm{ns}]}. \tag{24}$$

With the wavelength $\lambda \approx 0.086$ nm for the Mössbauer transition of ^{57}Fe, the separation between the neighbouring stroboscopic orders can be calculated to be $\varepsilon \approx 10.93$ mm/s. Note that this is the range of the hyperfine splitting in case of $\alpha - \mathrm{Fe}$ (outer line separation is 10.62 mm/s at room temperature), and the stroboscopic orders would only slightly overlap in case of a sample of low effective thickness in forward scattering. However, in case of grazing incidence near the critical angle of total external reflection due to the enhanced nuclear and electronic multiple scattering, the Mössbauer lines become extremely broad and a strong overlap of the stroboscopic orders is expected. This interference and partial overlap are manifested in rather complex resonance line shapes and an intriguing angular dependence of the delayed intensity in the various stroboscopic orders.

Both multilayers were prepared under ultra-high vacuum conditions by molecular beam epitaxy at the IMBL facility in IKS Leuven. The $[^{\mathrm{nat}}\mathrm{Fe}/^{57}\mathrm{Fe}]_{10}$ was prepared at room temperature onto a Zerodur glass substrate. The first layer and all other ^{57}Fe-layers were 95.5% isotopically enriched, and were grown from a Knudsen cell. The natural Fe layers, which have a ^{57}Fe-concentration of 2.17%, were grown from an electron gun source. The nominal layer thickness was 3.15 nm throughout the multilayer stack for both $^{\mathrm{nat}}$Fe and ^{57}Fe. Conversion electron Mössbauer spectra showed a pure $\alpha - \mathrm{Fe}$ spectrum. This spectrum was compared to a transmission Mössbauer spectroscopy spectrum of a natural iron calibration specimen, which was provided

by Amersham. Both hyperfine magnetic fields were fitted to be identical within the experimental error of 0.04%, and no sign of any second phase contamination was found.

Preparation and characterization of the MgO(001)/$[^{57}\mathrm{Fe/Cr}]_{20}$ multilayer sample has been described earlier (Bottyán *et al.*, 2002; Nagy *et al.*, 2002; Tanczikó *et al.*, 2004). The layering was verified as epitaxial and periodic, with thicknesses of 2.6 nm for the ^{57}Fe layer, and 1.3 nm for the Cr layer. SQUID magnetometry showed dominantly antiferromagnetic coupling between neighboring Fe layers. According to previous studies on this multilayer (Bottyán *et al.*, 2002; Nagy *et al.*, 2002; Tanczikó *et al.*, 2004), the magnetizations in Fe align to the [100] and [010] perpendicular easy directions in remanence, respectively corresponding to the [110] and $[\bar{1}10]$ directions of the MgO substrate. The layer magnetizations were aligned antiparallel in the consecutive Fe layers by applying a magnetic field (1.6 T) above the saturation value (0.96 T) in the Fe[010] easy direction of magnetization, and then releasing the field to remanence. This alignment is global, the antiferromagnetic domains were only different in the layer sequence of the parallel/antiparallel orientations (Nagy *et al.*, 2002).

3.1. Stroboscopic SMR on a $^{\mathrm{nat}}$Fe/^{57}Fe multilayer

Since in a $^{\mathrm{nat}}$Fe/^{57}Fe isotope-periodic multilayer the hyperfine field of ^{57}Fe is that of $\alpha - \mathrm{Fe}$ throughout the sample, this multilayer is particularly suitable for studying the modification of the resonance line shapes due to interference between nuclear and electronic scattering (Deák *et al.*, 1999; Deák *et al.*, 1994; Chumakov & Smirnov, 1991; Chumakov *et al.*, 1993). Fig. 2 shows results for the multilayer saturated in a transversal magnetic field of 50 mT. Panel *a* and *b* give the prompt electronic and delayed TISMR curves, respectively. The stroboscopic SMR spectra at the angles indicated by the arrows are given in panel *c* to *e*. The peak in the delayed reflectivity

at the total reflection angle in panel *b* is a special feature of SMR described earlier (Chumakov *et al.*, 1999; Deák *et al.*, 1994; Baron *et al.*, 1994). In panels *c* to *e*, the four resonance lines of the +1 and −1 stroboscopic orders (right and left sides, respectively) partially overlap with the 0^{th} order in the central part of the spectrum.

The delicate interplay between electronic and nuclear scattering is demonstrated by the considerable difference between the stroboscopic SMR spectra *c* to *e* in Fig. 2, which are taken at only slightly different grazing angles. In contrast to the symmetric forward scattering spectra (Callens *et al.*, 2002; Callens *et al.*, 2003), the stroboscopic SMR spectra are asymmetric due to the interference between the electronic and nuclear scattering. They also display both "absorption-like" and "dispersion-like" resonance line shape contributions. In case of decreased nuclear scattering strength and of the same electronic reflectivity (cf. panels *d* and *e* in Fig. 2), the signal to baseline ratio of the central part (heterodyne spectrum) decreases as compared to the signal to baseline ratio of stroboscopic orders ±1 in the spectrum wings.

The full lines are simultaneous least squares fits, using the theory outlined above and the computer code EFFI (Spiering *et al.*, 2000). The interference between nuclear and electronic scattering makes it possible to fit the layer structure in this isotope-periodic multilayer. The fitted value of the total thickness of pure $\alpha - \text{Fe}$ is 42.5 nm, comprised of nine times 1.49 nm of $^{\text{nat}}$Fe and 3.23 nm of ^{57}Fe, with 0.4 nm common roughness at the interfaces. In order to achieve the simultaneous fit, displayed by the full line in Figure 2, we had to assume that half a bilayer on top and bottom ($^{\text{nat}}$Fe and ^{57}Fe, respectively) was modified. The transversal hyperfine magnetic field was fixed to 33.08 T in the nine ^{57}Fe/$^{\text{nat}}$Fe bi-layers in the middle of the multilayer, which is the room temperature value for $\alpha - \text{Fe}$.

3.2. Stroboscopic SMR of an antiferromagnetic ^{57}Fe/Cr multilayer

Fig. 3 and Fig. 4 display similar sets of spectra of an ^{57}Fe/Cr antiferromagnetically coupled epitaxial multilayer on MgO(001). The dots are the experimental data points, while the continuous lines are simultaneous fits to a model structure of $\left[^{57}\mathrm{Fe}\,(2.6\ \mathrm{nm})\,/\,\mathrm{Cr}\,(1.3\ \mathrm{nm})\right]_{20}$, based on the respective theory.

Non-resonant reflectivity, TISMR and stroboscopic SMR spectra were recorded first with the Fe layer magnetizations parallel/antiparallel (Fig. 3) to the $k-$vector of the SR beam. The stroboscopic spectra were taken at the angles of total reflection (c), at the antiferromagnetic (d) and at the structural Bragg peak (e) positions. After this, a magnetic field of 20 mT was applied to the multilayer in longitudinal direction. This is known to flop the magnetizations to the perpendicular Fe(010) easy axis of the magnetization (Bottyán *et al.*, 2002; Tanczikó *et al.*, 2004). Non-resonant reflectivity, TISMR and stroboscopic SMR spectra at the same angular positions were again collected (Fig. 4).

The major difference between Figs. 3 and 4 is the presence, respectively absence, of the AF Bragg peak in the delayed reflectivity curve b. This antiferromagnetic alignment, i.e., the longitudinal hyperfine field of alternating sign in consecutive Fe layers, is justified by the simultaneous fit in Fig. 3. In Fig. 4, the fitted Fe magnetizations are perpendicular to the wave vector of the SR. Indeed, the scattering amplitudes depend on the angle of the wave vector and the direction of the hyperfine magnetic field. In the case of perpendicular orientation, this angle is 90 degrees for consecutive layer magnetizations and no AF contrast can be observed. In case of parallel/anti–parallel orientations, however, the angles with respect to the wave vector of SR are 0 and 180 degrees, respectively. Therefore, the hyperfine contrast is present and the AF Bragg peak is visible in panel b of Fig. 3.

The count rate at the baseline of a stroboscopic SMR spectrum, measured at a cer-

tain grazing angle θ, is closely related to the TISMR spectrum at this angle. Therefore, the respective experimental count rates of the stroboscopic SMR spectrum at the AF Bragg peak positions (panel d) differ by almost two orders of magnitude. Spectrum 3d is also the only spectrum for which no considerable enhanced dynamic broadening can be observed.

Note that, in panels d, the zeroth order resonances are considerably enhanced with respect to the ± 1 order stroboscopic resonances. This can be explained by an enhanced radiative coupling of the samples. Since the radiative coupling does not contribute to the ± 1 order stroboscopic resonances, it only influences the baseline and the central resonances.

At the multilayer Bragg reflections (panel e), and at the total reflection peak (panel c), the suppression of the higher stroboscopic orders is much smaller, which means that the radiative coupling term is not dominating here. These spectra also show a left/right asymmetry due to the variation of the phase of the total scattering amplitude with energy. This latter allows for phase determination of the scattering amplitude from a set of stroboscopic SMR spectra, which work will be published later.

4. Summary

In summary, the concept of heterodyne/stroboscopic detection of nuclear resonance scattering was outlined for a general scattering channel, with special emphasis on the grazing incidence reflection case. In any non-forward scattering channel, the electronic scattering influences the NRS spectral shape, while in forward scattering, this is a mere multiplicative factor. The interplay between electronic and nuclear scattering, as a function of the scattering angle, facilitates the determination of the electronic and nuclear scattering amplitudes. The code of the present theory has been merged into the EFFI program (Spiering *et al.*, 2000), and was used in simultaneous data fitting

of x-ray reflectivity, time integral reflectivity and stroboscopic SMR spectra. Similar to time differential SMR, stroboscopic SMR spectra have been shown to be sensitive to the direction of the hyperfine fields of the individual layers. Therefore, it is possible to apply this method to the study of magnetic multilayers and thin films. The experiments on $\left[^{57}\mathrm{Fe}\,(2.6\ \mathrm{nm})\,/\mathrm{Cr}\,(1.3\ \mathrm{nm})\right]_{20}$ and $\left[^{\mathrm{nat}}\mathrm{Fe}/^{57}\mathrm{Fe}\right]_{10}$ multilayers demonstrated that stroboscopic detection of synchrotron Mössbauer reflectometry of ^{57}Fe-containing thin films is feasible in dense bunch modes, which are not necessarily suitable for time differential nuclear resonance scattering experiments on ^{57}Fe.

References

Afanasev, A. M. & Kagan, Y. (1964). *Sov. Phys. JETP*, **18**, 1139–1149.

Baron, A. Q. R., Arthur, J., Ruby, S. L., Chumakov, A. I., Smirnov, G. V. & Brown, G. S. (1994). *Phys. Rev. B*, **50**, 10354–10357.
URL: *http://link.aps.org/doi/10.1103/PhysRevB.50.10354*

Blume, M. & Kistner, O. C. (1968). *Phys. Rev.* **171**(2), 417–425.

Bottyán, L., Deák, L., Dekoster, J., Kunnen, E., Langouche, G., Meersschaut, J., Major, M., Nagy, D. L., Rüter, H. D., Szilágyi, E. & Temst, K. (2002). *Journal of Magnetism and Magnetic Materials*, **240**(13), 514 – 516. 4th International Symposium on Metallic Multilayers.
URL: *http://www.sciencedirect.com/science/article/pii/S0304885301008940*

Callens, R., Coussement, R., Kawakami, T., Ladrière, J., Nasu, S., Ono, T., Serdons, I., Vyvey, K., Yamada, T., Yoda, Y. & Odeurs, J. (2003). *Phys. Rev. B*, **67**, 104423.
URL: *http://link.aps.org/doi/10.1103/PhysRevB.67.104423*

Callens, R., Coussement, R., L'abbé, C., Nasu, S., Vyvey, K., Yamada, T., Yoda, Y. & Odeurs, J. (2002). *Phys. Rev. B*, **65**, 180404.
URL: *http://link.aps.org/doi/10.1103/PhysRevB.65.180404*

Chumakov, A. I., Niesen, L., Nagy, D. L. & Alp, E. E. (1999). *Hyperfine Interactions*, **123-124**(1-4), 427–454.
URL: *http://dx.doi.org/10.1023/A:1017028024642*

Chumakov, A. I. & Smirnov, G. V. (1991). *JETP Lett*, **53**(5), 271 – 275.

Chumakov, A. I., Smirnov, G. V., Baron, A. Q. R., Arthur, J., Brown, D. E., Ruby, S. L., Brown, G. S. & Salashchenko, N. N. (1993). *Phys. Rev. Lett.* **71**, 2489–2492.
URL: *http://link.aps.org/doi/10.1103/PhysRevLett.71.2489*

Coussement, R., Cottenier, S. & L'abbé, C. (1996). *Phys. Rev. B*, **54**, 16003–16009.
URL: *http://link.aps.org/doi/10.1103/PhysRevB.54.16003*

Deák, L., Bayreuther, G., Bottyán, L., Gerdau, E., Korecki, J., Kornilov, E. I., Lauter, H. J., Leupold, O., Nagy, D. L., Petrenko, A. V. *et al.* (1999). *Journal of applied physics*, **85**(1), 1–7.

Deák, L., Bottyán, L., Major, M., Nagy, D. L., Spiering, H. & Szilágyi, E. (1999). In *Condensed matter studies by nuclear methods: proceedings of XXXIV Zakopane School of Physics*, edited by E. A. Görlich & A. T. Pędziwiatr, pp. 151–161. Kraków: Wydawnictwo Uniwersytetu Jagiellońskiego.
URL: *http://books.google.hu/books?id=FlwdAQAACAAJ*

Deák, L., Bottyán, L., Major, M., Nagy, D. L., Spiering, H., Szilágyi, E. & Tanczikó, F. (2002). *Hyperfine Interactions*, **144/145**, 45–52.

Deák, L., Bottyán, L. & Nagy, D. L. (1994). *Hyperfine Interactions*, **92**(1), 1083–1088.
URL: *http://dx.doi.org/10.1007/BF02065737*

Deák, L., Bottyán, L., Nagy, D. L. & Spiering, H. (1996). *Phys. Rev. B*, **53**, 6158–6164.
URL: *http://link.aps.org/doi/10.1103/PhysRevB.53.6158*

Deák, L., Bottyán, L., Nagy, D. L. & Spiering, H. (2001). *Physica B*, **297**, 113–117.

Gerdau, E. & DeWaard, H. (1999). *Hyperfine Interactions*, **123-124**(1-4), 0–0.
URL: *http://dx.doi.org/10.1023/A%3A1017073002352*

Hannon, J. P., Hung, N. V., Trammell, G. T., Gerdau, E., Mueller, M., Rüffer, R. & Winkler, H. (1985*a*). *Phys. Rev. B*, **32**, 5068–5080.
URL: *http://link.aps.org/doi/10.1103/PhysRevB.32.5068*

Hannon, J. P. & Trammell, G. T. (1968). *Phys. Rev.* **169**, 315–329.
URL: *http://link.aps.org/doi/10.1103/PhysRev.169.315*

Hannon, J. P. & Trammell, G. T. (1969). *Phys. Rev.* **186**, 306–325.

Hannon, J. P., Trammell, G. T., Mueller, M., Gerdau, E., Rüffer, R. & Winkler, H. (1985*b*). *Phys. Rev. B*, **32**, 6363–6373.
URL: *http://link.aps.org/doi/10.1103/PhysRevB.32.6363*

Irkaev, S. M., Andreeva, M. A., Semenov, V. G., Belozerskii, G. N. & Grishin, O. V. (1993). *Nuclear Instruments and Methods in Physics Research Section B: Beam Interactions with Materials and Atoms*, **74**(4), 554 – 564.
URL: *http://www.sciencedirect.com/science/article/pii/0168583X93959555*

Kagan, Y. & Afanasev, A. M. (1964). *Zh. Eksperim. i Teor. Fiz.* **47**, 1108–.

L'abbé, C., Coussement, R., Odeurs, J., Alp, E. E., Sturhahn, W., Toellner, T. S. & Johnson, C. (2000). *Phys. Rev. B*, **61**, 4181–4185.
URL: *http://link.aps.org/doi/10.1103/PhysRevB.61.4181*

Lax, M. (1951). *Rev. Mod. Phys.* **23**(4), 287–310.

Nagy, D. L., Bottyán, L., Croonenborghs, B., Deák, L., Degroote, B., Dekoster, J., Lauter, H. J., Lauter-Pasyuk, V., Leupold, O., Major, M., Meersschaut, J., Nikonov, O., Petrenko, A., Rüffer, R., Spiering, H. & Szilágyi, E. (2002). *Phys. Rev. Lett.* **88**(15), 157202.

Nagy, D. L., Bottyán, L., Deák, L., Dekoster, J., Langouche, G., Semenov, V. G., Spiering, H. & Szilágyi, E. (1999). In *Mössbauer Spectroscopy in Materials Science*, edited by M. Miglierini & D. Petridis, NATO ASI series. Series C. Mathematical and physical sciences, pp. 323–336. Netherlands: Kluwer Academic Publishers.
URL: *http://books.google.hu/books?id=r8LaY6br5XUC*

Röhlsberger, R. (1999). *Hyperfine Interactions*, **123-124**(1-4), 455–479.
URL: *http://dx.doi.org/10.1023/A%3A1017075907804*

Röhlsberger, R. (2005). In *Nuclear Condensed Matter Physics with Synchrotron Radiation*, vol. 208 of *Springer Tracts in Modern Physics*, pp. 1–6. Springer Berlin Heidelberg.
URL: *http://dx.doi.org/10.1007/978-3-540-44699-6_1*

Röhlsberger, R., Bansmann, J., Senz, V., Jonas, K. L., Bettac, A., Meiwes-Broer, K. H. & Leupold, O. (2003). *Phys. Rev. B*, **67**, 245412.
URL: *http://link.aps.org/doi/10.1103/PhysRevB.67.245412*

Röhlsberger, R., Schlage, K., Sahoo, B., Couet, S. & Rüffer, R. (2010). *Science*, **328**(5983), 1248–1251.
URL: *http://www.sciencemag.org/content/328/5983/1248.abstract*

Röhlsberger, R., Wille, H.-C., Schlage, K. & Sahoo, B. (2012). *Nature*, **482**(7384), 199–203.
URL: *http://dx.doi.org/10.1038/nature10741*

Serdons, I., Nasu, S., Callens, R., Coussement, R., Kawakami, T., Ladrière, J., Morimoto, S., Ono, T., Vyvey, K., Yamada, T., Yoda, Y. & Odeurs, J. (2004). *Phys. Rev. B*, **70**, 014109.
URL: *http://link.aps.org/doi/10.1103/PhysRevB.70.014109*

Sladecek, M., Sepiol, B., Kaisermayr, M., Korecki, J., Handke, B., Thiess, H., Leupold, O., Rüffer, R. & Vogl, G. (2002). *Surface Science*, **507510**(0), 124 – 128.
URL: *http://www.sciencedirect.com/science/article/pii/S0039602802011871*

Smirnov, G. V., van Bürck, U., Chumakov, A. I., Baron, A. Q. R. & Rüffer, R. (1997). *Phys. Rev. B*, **55**, 5811–5815.
URL: *http://link.aps.org/doi/10.1103/PhysRevB.55.5811*

Spiering, H., Deák, L. & Bottyán, L. (2000). *Hyp. Int.* **125**, 197–204. The computer program EFFI is available from `ftp://nucssp.rmki.kfki.hu/effi` including the experimental data.

Sturhahn, W. & Gerdau, E. (1994). *Phys. Rev. B*, **49**, 9285–9294.
URL: *http://link.aps.org/doi/10.1103/PhysRevB.49.9285*

Tanczikó, F., Deák, L., Nagy, D. L. & Bottyán, L. (2004). *Nuclear Instruments and Methods in Physics Research Section B: Beam Interactions with Materials and Atoms*, **226**(3), 461 – 467.
URL: *http://www.sciencedirect.com/science/article/pii/S0168583X04008481*

Yoda, Y., Yabashi, M., Izumi, K., Zhang, X., Kishimoto, S., Kitao, S., Seto, M., Mitsui, T., Harami, T., Imai, Y. & Kikuta, S. (2001). *Nuclear Instruments and Methods in Physics Research Section A: Accelerators, Spectrometers, Detectors and Associated Equipment*, **467/468,Part1**(0), 715–718. 7th Int.Conf. on Synchrotron Radiation Instrumentation.
URL: *http://www.sciencedirect.com/science/article/pii/S0168900201004740*

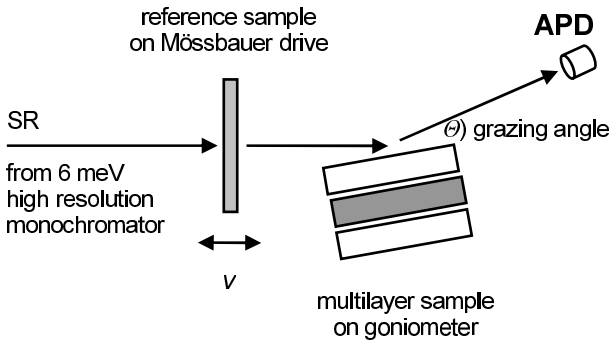

Fig. 1. Experimental setup for stroboscopic Synchrotron Mössbauer Reflectometry.

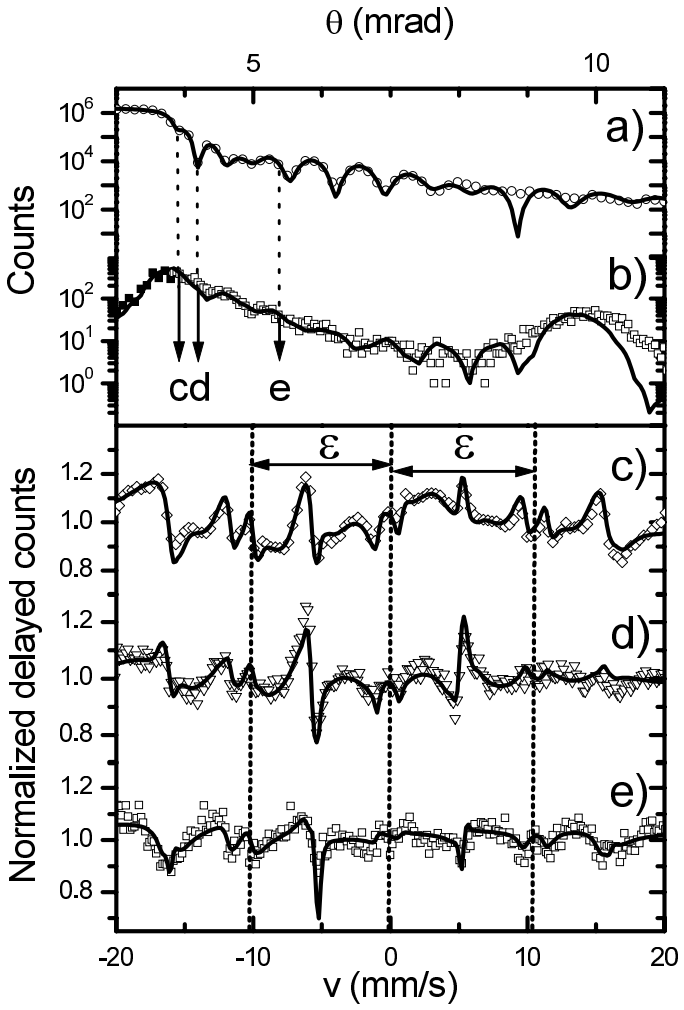

Fig. 2. Prompt electronic (a) and delayed nuclear reflectivity (b) curves as well as stroboscopic SMR spectra (c) to e), of a $\left[^{\mathrm{nat}}\mathrm{Fe}/^{57}\mathrm{Fe}\right]_{10}$ isotopic multilayer at grazing angles indicated by the arrows. Vertical dotted lines in panels c) to e) indicate the center of the zero and ± 1 order stroboscopic bands separated by $\varepsilon \approx 10.93$ mm/s for the applied observation window period.

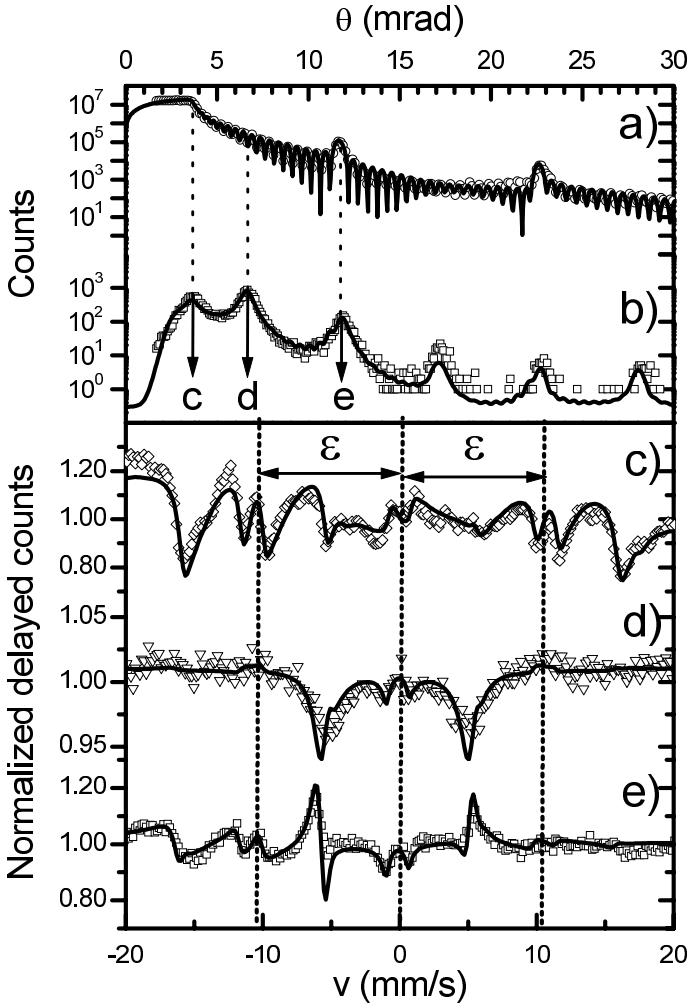

Fig. 3. Prompt electronic (a) and delayed nuclear (b) reflectivity curves as well as stroboscopic SMR spectra (c to e) of a MgO(001)/ $[^{57}\mathrm{Fe/Cr}]_{20}$ antiferromagnetic multilayer at various angles indicated by arrows in b). The consecutive Fe layer magnetizations are aligned parallel/antiparallel with to the SR beam. Vertical dotted lines in panels c) to e) indicate the center of the zero and ±1 order stroboscopic bands separated by $\varepsilon \approx 10.93$ mm/s for the applied observation window period.

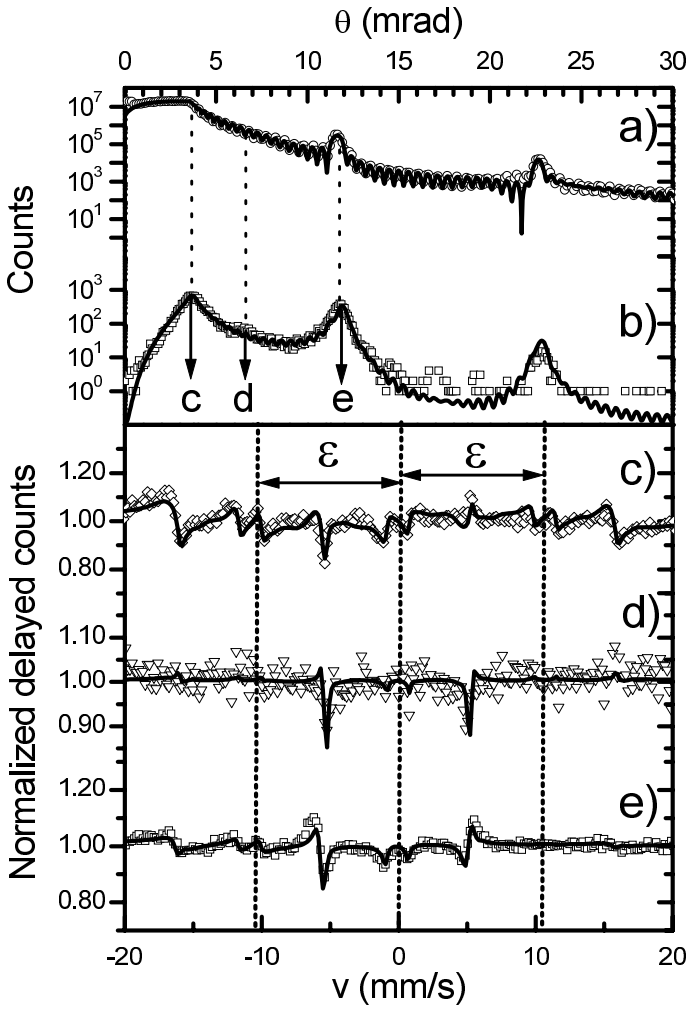

Fig. 4. Prompt electronic (a) and delayed nuclear (b) reflectivity curves as well as stroboscopic SMR spectra (c to e) of a $\left[^{57}\mathrm{Fe}\,(2.6\,\mathrm{nm})\,/\mathrm{Cr}\,(1.3\,\mathrm{nm})\right]_{20}$/MgO antiferromagnetic multilayer at various angles indicated by arrows. The consecutive Fe layer magnetizations are aligned perpendicular to the SR beam. Vertical dotted lines in panels c) to e) indicate the center of the zero and ± 1 order stroboscopic bands separated by $\varepsilon \approx 10.93$ mm/s for the applied observation window period.

Synopsis

The theory of heterodyne/stroboscopic detection of nuclear resonance scattering is developed for various dynamical scattering channels. The grazing incidence case is discussed in detail and is experimentally demonstrated on magnetic multilayers.